NASA TECHNICAL MEMORANDUM

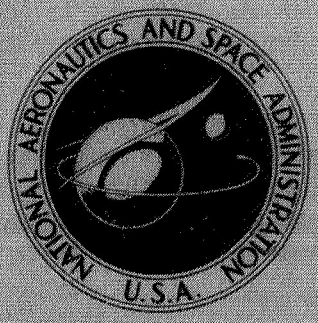

NASA TM X-2092

NASA TM X-2092

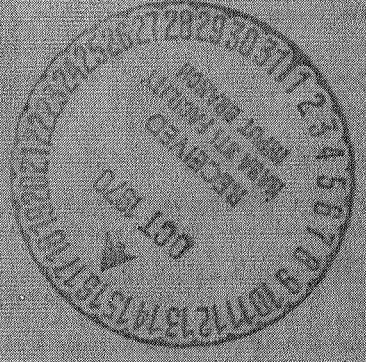

ANALYSIS OF BENDING LOADS OF HYPERSONIC AIRCRAFT

by Mark D. Ardema
Office of Advanced Research and Technology
Mission Analysis Division
Moffett Field, Calif. 94035

NATIONAL AERONAUTICS AND SPACE ADMINISTRATION • WASHINGTON, D. C. • OCTOBER 1970

1. Report No.	2. Government Accession No.	3. Recipient's Catalog No.
NASA TM X-2092		

4. Title and Subtitle	5. Report Date
ANALYSIS OF BENDING LOADS OF HYPERSONIC AIRCRAFT	October 1970
	6. Performing Organization Code

7. Author(s)	8. Performing Organization Report No.
Mark D. Ardema	A-3625
	10. Work Unit No.
9. Performing Organization Name and Address	789-50-01-01-15
Office of Advanced Research and Technology Mission Analysis Division Moffett Field, California 94035	11. Contract or Grant No.
	13. Type of Report and Period Covered
12. Sponsoring Agency Name and Address	Technical Memorandum
National Aeronautics and Space Administration Washington, D. C. 20546	14. Sponsoring Agency Code

15. Supplementary Notes

16. Abstract

The longitudinal bending moments on all-body configurations and wing-body configurations of a hypersonic aircraft are determined and compared. Bending-moment distributions are determined from idealized vehicle loadings due to a static maneuver, a dynamic gust condition, and a dynamic landing impact. Characteristics of selected nominal configurations are discussed, and parametric data are given that relate bending-moment magnitude to design laod criteria and configuration parameters. The results indicate that for the nominal design load criteria there is no appreciable difference in the magnitude of the bending moments on the two nominal configurations. The maneuver and landing loads are found to be dominant for both the all-body and the wind-body configurations.

17. Key Words (Suggested by Author(s))	18. Distribution Statement
Bending loads Hypersonic aircraft	Unclassified – Unlimited

19. Security Classif. (of this report)	20. Security Classif. (of this page)	21. No. of Pages	22. Price*
Unclassified	Unclassified	30	$3.00

*For sale by the Clearinghouse for Federal Scientific and Technical Information
Springfield, Virginia 22151

SYMBOLS

$A,B,E,Q,$ G,H,J	constants defined by equations (A7) and (A8)
C	center of gravity, ft
C_{L_α}	lift curve slope, 1/deg
C_{MG}	damping constant of main gear, lb sec/ft
C_{NG}	damping constant of nose gear, lb sec/ft
C_P	body center of pressure, ft
g	acceleration due to gravity, ft/sec^2
h_{z_1}	unit step applied at $Z = Z_1$
K	radius of gyration, ft
K_{G_i}	constants of integration of gust motion
K_{MG}	spring constant of main gear, lb/ft
K_{NG}	spring constant of nose gear, lb/ft
L	lift force, lb
l	length, ft
M	bending moment, ft-lb
M_{PEAK}	peak bending moment, ft-lb
N	bending moment dependent upon load condition, ft-lb
n	maneuver load factor
q	dynamic pressure, lb/ft^2
S	plan area, ft^2
t	time, sec
V	vehicle velocity in gust, fps

V_g	gust velocity, fps
V_S	landing sink speed, fps
W	weight, lb
x	body station, ft
y	height of vehicle c.g., ft
α	angle of attack, deg
δ	control surface deflection, deg
δ_g	gust deflection, rad

Subscripts

B	body
C	canard
G	gust
i = M,L, or G	
L	landing
M	maneuver
P	propulsion system
P_1	inlet
P_2	nozzle
π	breakpoint
T	tail
x	ahead of station x
o	initial value

ANALYSIS OF BENDING LOADS OF HYPERSONIC AIRCRAFT

Mark D. Ardema

Office of Advanced Research and Technology
Mission Analysis Division
Moffett Field, California 94035

SUMMARY

The longitudinal bending moments on all-body configurations and wing-body configurations of a hypersonic aircraft are determined and compared. Bending-moment distributions are determined from idealized vehicle loadings due to a static maneuver, a dynamic gust condition, and a dynamic landing impact. Characteristics of selected nominal configurations are discussed, and parametric data are given that relate bending-moment magnitude to design load criteria and configuration parameters. The results indicate that for the nominal design load criteria there is no appreciable difference in the magnitude of the bending moments on the two nominal configurations. The maneuver and landing loads are found to be dominant for both the all-body and the wing-body configurations.

INTRODUCTION

Recent studies of liquid-hydrogen-fueled hypersonic aircraft have considered configurations in which the vehicle wing and body are blended together (blended body) or in which there is no wing at all (all body). Such configurations are of interest primarily because of their high volumetric efficiency, and possibly superior engine-airframe integration characteristics when compared with conventional wing-body configurations. Comparative mission performance analyses of all-body and wing-body configurations have therefore been initiated. In support of these analyses, a study of vehicle loads and weights was undertaken. The first part of this study, covered in this report, is concerned with vehicle loads.

The purpose of the loads study was to compare the loading characteristics of representative all-body and wing-body configurations. Since the former is a significant departure from conventional aircraft configurations, many of the empirical data from existing aircraft designs are not applicable for estimation of the vehicle loads of this configuration. Therefore, the method used in the study is an analytical one based on simplified vehicle and vehicle loading models. Insofar as possible, the same analysis methods and assumptions were applied to both vehicles. Characteristics of selected nominal configurations are discussed, and parametric data relating vehicle loading to design load criteria and configuration parameters are presented.

This report is concerned exclusively with determination of longitudinal bending moments. Historically it has been a fair assumption that the body structural weight of wing-body configurations is affected primarily by longitudinal bending moments. For the all-body vehicle there

may be some second-order effects. In particular, the large body span at the rear leads to transverse bending moments that may be sufficiently large to affect the body weight, and it is necessary to account for this factor in determining the body weight.

Since the ultimate goal of the loads analysis is to obtain vehicle body structural weight, the relationship between body structural weight and loading should be mentioned. Aircraft body structure is generally buckling-critical, and simplified buckling analysis shows, to a first approximation, that body structural weight is proportional to the square root of bending moment.

METHOD OF ANALYSIS

The nominal configurations chosen for the study are shown in figure 1. The all-body vehicle (fig. 1(a)) consists of an elliptical cone forebody and an afterbody of elliptical cross section, which fairs to a straight line trailing edge. The wing-body vehicle (fig. 1(b)) consists of a double-ended power-law body, a delta wing, and an aft tail. Both configurations are assumed to have a gross take-off weight of 500,000 lb and a body volume of 71,400 ft^3.

Vehicle loading was determined by station-by-station analysis (described in the appendix). Loads due to a static maneuver, a dynamic gust condition, and a dynamic landing impact were computed for a simplified vehicle loading model; and the envelope of the maximum absolute values of the longitudinal bending moment was computed. The nominal design load criteria for the three loading conditions were: a 2.5 load factor maneuver, a 10-fps sink speed landing, and a 50-fps vertical gust encountered at a flight speed of 750 fps. These values are typical of the design load criteria of current transport aircraft. Nominal vehicle weight is gross take-off weight for the maneuver and gust conditions and 75 percent of this value for the landing condition.

RESULTS

Nominal Bending Moments

Figure 2 shows bending moment (absolute value) as a function of body station for the two nominal configurations. For the all-body (fig. 2(a)) and wing-body (fig. 2(b)) configurations, the maneuver and landing conditions are the dominant design conditions. The gust condition results in lower vehicle loadings. The two peaks on the landing curves are due to impact of the nose gear (forward peak) and to the subsequent peak main gear reaction (fig. 17). The middle peak on the wing-body landing curve, as well as the forward peak, is due to nose gear impact and is actually a negative bending moment. (The dynamics of the landing motion are discussed in the appendix.) Since the maneuver loads depend largely on differences in longitudinal lift and weight distribution, the loading on both configurations could be reduced by improving the longitudinal weight distribution within the body. The severity of the peaks on the wing-body landing curve is due primarily to the relatively long length of this vehicle and indicates the desirability of introducing the landing loads more uniformly into the body, for example, by the use of the multiple main gears. A comparison of figures 2(a) and 2(b) shows that the magnitude of the peak bending moment on each of the two configurations is essentially the same.

Design Criteria Variations

The effects of design criteria variations on vehicle loading are shown in figures 3 through 6. The maneuver bending-moment distributions for four values of load factor are shown in figures 3(a) and 3(b), with $n = 1.0$ corresponding to the cruise condition. It is seen that incremental changes in the load factor result in proportional changes in bending moment. Figure 4 shows that the variation of landing bending moment is relatively insensitive to sink speed. The curve labeled 0 fps corresponds to the prelanding trim condition. Figure 5 shows that gust bending moment is closely proportional to gust velocity; again, 0 fps is the cruise condition. Note that for the range of parameters considered, maneuver and gust loads are higher and landing loads lower for the all-body than for the wing-body configuration.

The peak bending moments as a function of the ratio of the design load weight to gross take-off weight for each loading condition are shown in figure 6. The circles indicate the nominal value of the ratio for each loading condition. All these curves are very nearly linear. The wing-body curves have higher slopes, indicating a higher sensitivity to the weight ratio. The maneuver and gust load curves are only of academic interest because the gross take-off weight condition must always be considered for these loading conditions. The landing curve indicates the relationship between loading and design landing weight. In particular, figure 6(b) indicates that vehicle loading on the longer wing-body configuration would be substantially increased if this vehicle were required to land at its gross take-off weight.

Shape and Size Variations

All-body configuration– It was found that variations in vehicle shape and size influence primarily the magnitude of the bending-moment envelope. For this reason, the effects of shape and size variations were considered in terms of the peak bending moment, which is indicative of the changes in overall loading. Figures 7 through 9 show the sensitivity of peak bending moment to the three parameters that describe the shape of the all-body configuration – breakpoint ratio, body sweep, and fatness ratio. The parameters are defined in figure 7 and their nominal value is indicated by tick marks on each figure. The nominal shape is not necessarily optimum and served only as a base about which the shape variations were made.

Figure 7 shows the effect of variations of breakpoint ratio on the peak bending moment for each of the three loading conditions. The maneuver and landing load curves have slopes of approximately equal magnitude and opposite signs. Changes in the breakpoint ratio are expected to have a small net effect on the body structural weight.

The effect of body sweep is shown in figure 8. At higher values of sweep (greater vehicle length), the peak bending moments become increasingly larger, particularly for the landing condition. Although high sweeps may be expected to result in high body weights, high-sweep vehicles have attractive hypersonic aerodynamic performance and therefore are of interest.

The peak bending moment decreases as fatness ratio increases (fig. 9); thus, body structural weight may be expected to decrease with increasing fatness ratio. Aerodynamic efficiency, however, decreases as fatness ratio increases; therefore, fatness ratio is important in configuration optimization.

Figure 10 shows the effect of size on the all-body vehicle peak maneuver bending moment. The size variation was made with the shape parameters held constant at their nominal values. The tick mark indicates the gross weight and density for the nominal vehicle. Possible values of gross vehicle density (defined as gross take-off weight divided by body volume) for liquid-hydrogen-fueled hypersonic vehicles are covered by the three curves shown in figure 10. These densities are lower than those for current transport aircraft (about 10 to 25 lb/ft^3) because of the low density of hydrogen fuel (about 4.5 lb/ft^3). As expected, the peak bending moment increases at an increasing rate with gross take-off weight. The curves of constant density are in excellent agreement with the relationship $M_{PEAK} \sim W_{TO}^{4/3}$, which can be obtained by a simplified analysis. It should be noted that the wing loading is referenced to body planform area; therefore, wing loading cannot be held constant for this variation of the configuration. The variation of wing loading with gross weight and density is shown at the top of figure 10.

Wing-body configuration– The shape parameters for this vehicle are fineness ratio (length/diameter), exponent of the power law which defines body shape, and wing loading. The ticks in figures 11 through 13 indicate the nominal values of these parameters. The first shape variation, that of body fineness ratio, is shown in figure 11, which indicates the usual trend of nearly linear increases in loading with increases in fineness ratio. Fineness ratio also has a strong influence on aerodynamic efficiency and is thus an important parameter for configuration optimization.

Figure 12 shows the effect on the peak bending moment of the exponent of the power law that defines body shape, which varies from a cylinder (exponent = 0) to a double-ended cone (exponent = 1). Since the distributed weight of the body contents shifts toward the vicinity of the wing as the exponent is increased, the maneuver and gust loads decrease, while the landing load remains essentially constant. However, the diameter near the middle of the body increases as the exponent is increased. As a result, the body can more easily resist bending and its weight should be decreased.

The effect of varying take-off wing loading is shown in figure 13. The predominant effect of increasing wing loading (decreasing wing area) is that the body carries an increasingly larger percentage of the lift. This results in more compatible longitudinal lift and weight distributions and causes the maneuver and gust loads to decrease. Again, however, the landing loads remain approximately constant and no significant changes in body weight are expected. Of course there will be large changes in wing weight with changes in wing loading. It is seen that for the ranges of the shape parameters considered, the all-body loads have larger variations (figs. 7 through 9) than do the wing-body loads (figs. 11 through 13).

Figure 14 shows the effect of size on the wing-body peak maneuver bending moment for the same three densities considered for the all-body vehicles. This variation was made with fixed body shape and fixed wing loading. A comparison of figures 10 and 14 shows the effect of increasing gross take-off weight with fixed density to be almost identical for both vehicles. The effect of density changes (i.e., volume) is seen to be relatively small for the wing-body configuration as compared to the all-body.

CONCLUSIONS

The longitudinal bending moments on all-body and wing-body configurations have been determined and compared. It was found that for the nominal design conditions there is no appreciable difference in the magnitude of the bending moments of the two nominal configurations. Maneuver and landing loads are the dominant design loads for the all-body and wing-body configurations. For both, incremental changes in the design load conditions result in proportional incremental changes in maneuver and gust loads, while landing loads are rather insensitive to design landing sink speed. The most influential shape parameter for the all-body vehicle was found to be body sweep, while fineness ratio was the most influential shape parameter for the wing-body vehicle. The effect of size on the loads is similar for both configurations, that is, the peak bending moment increases rapidly as gross take-off weight increases; however, the all-body bending moments are more sensitive to gross aircraft density.

National Aeronautics and Space Administration
Moffett Field, Calif., 94035, April 24, 1970

APPENDIX

BENDING MOMENT ANALYSIS

For both the all-body and wing-body vehicles, the vehicle loads are obtained by simulating vehicle pitch-plane motion during maneuvers, gusts, and landings. Simplified vehicle loading models are used in which it is assumed that: (1) lift forces are distributed uniformly over plan area, (2) body weight is distributed uniformly over body volume, (3) control surface forces and landing gear reactions are point loads, and (4) propulsion system weight is uniformly distributed. For the wing-body vehicle, the wing and body lifting forces are determined independently. The resulting one-dimensional loading models are shown in figure 15. All lift forces are assumed to be linear functions of angle of attack. Longitudinal bending moments were computed for each of the three loading conditions and the envelope of the maximum values taken as the design loading condition. Since the computations for the all-body and the wing-body are very similar, only the all-body computation will be described in detail.

For each loading condition, the all-body vehicle was first trimmed with the canard. The necessary canard deflection δ_{C_i} and vehicle $(C_{L_\alpha} q)_i$ were computed from:

$$\left.\begin{aligned} \delta_{C_i} &= -\frac{S_B \alpha_{o_i}[C_i - (2/3)\ell_B] + S_T(\alpha_{o_i} + \delta_{T_i})(C_i - \ell_T)}{S_C(C_i - \ell_C)} - \alpha_{o_i} \\ (C_{L_\alpha} q)_i &= \frac{W_i}{S_B \alpha_{o_i} + S_C(\alpha_{o_i} + \delta_{C_i}) + S_T(\alpha_{o_i} + \delta_{T_i})} \end{aligned}\right\} \quad \text{(A1)}$$

where quantities with subscript i depend on the loading condition. By assumption (1) above, the center of pressure is at two thirds of the vehicle length. The equations of motion are then solved for the landing and gust conditions. The bending-moment distribution is computed at small time intervals from:

$$\begin{aligned} M_i(x,t) = {} & h_{L_C} L_{C_i}(x - \ell_C) + L_{B x_i}(x - C_{P x_i}) + h_{L_T} L_{T_i}(x - \ell_T) \\ & - W_{x_i}(x - C_{x_i}) - \frac{W_{x_i} \ddot{\alpha}_i}{g}\left[K_{x_i}^2 + \left(\frac{\ddot{y}_i}{\ddot{\alpha}_i} + C_i - C_{x_i}\right)(x - C_{x_i})\right] + N_i \end{aligned} \quad \text{(A2)}$$

where

$$W_{x_i} = W_{Bx_i} + W_{Px} + h_{L_C} W_C + h_{L_T} W_T$$

$$C_{x_i} = \frac{1}{W_{x_i}} \left(W_{Bx_i} C_{Bx_i} + W_{Px} C_{Px} + h_{L_C} W_C l_C + h_{L_T} W_T l_T \right)$$

$$K_{x_i}^2 = \frac{1}{W_{x_i}} \left\{ W_{Bx_i} \left[K_{Bx_i}^2 + (C_{Bx_i} - C_{x_i})^2 \right] + h_{L_C} W_C (l_C - C_{x_i})^2 \right.$$

$$\left. + W_{Px} \left[K_{Px}^2 + (C_{Px} - C_{x_i})^2 + h_{L_T} W_T (l_T - C_{x_i})^2 \right] \right\}$$

$$W_{Bx_i} = \begin{cases} \dfrac{2x^3 W_{B_i}}{l_B l_\pi (l_B + l_\pi)} , & 0 < x < l_\pi \\ \dfrac{(3 l_B x^2 - 2x^3 - l_\pi^2 l_B) W_{B_i}}{l_B (l_B^2 - l_\pi^2)} , & l_\pi < x < l_B \end{cases}$$

$$C_{Bx_i} = \begin{cases} \dfrac{3}{4} x , & 0 < x < l_\pi \\ l_\pi + \dfrac{(x - l_\pi)(l_\pi + l_B)}{2(2l_\pi + l_B)} - \left[\dfrac{l_\pi}{2(l_\pi + l_B)} + \dfrac{(x - l_\pi)}{(2l_\pi + l_B)} \right] \dfrac{W_{B_i} l_\pi^2}{W_{Bx_i} l_B} , & l_\pi < x < l_B \end{cases}$$

$$K_{Bx_i}^2 = \begin{cases} \dfrac{3}{80} x^2 , & 0 < x < l_\pi \\ \dfrac{2 l_\pi^2 W_{B_i}}{l_B (l_B + l_\pi) W_{Bx_i}} \left[\dfrac{3}{80} l_\pi^2 + \left(\dfrac{3}{4} l_\pi - C_{Bx_i} \right)^2 \right] + \left[1 - \dfrac{2 l_\pi^2 W_{B_i}}{l_B (l_\pi + l_B) W_{Bx_i}} \right] \\ \cdot \left\{ \dfrac{(x - l_\pi)^2}{10} \dfrac{(2l_\pi + 3l_B)}{(2l_\pi + l_B)} - \left[\dfrac{(x - l_\pi)(l_\pi + l_B)}{2(2l_\pi + l_B)} \right]^2 \right. \\ \left. + \left[l_\pi + \dfrac{(x - l_\pi)(l_\pi + l_B)}{2(2l_\pi + l_B)} - C_{Bx_i} \right]^2 \right\} , & l_\pi < x < l_B \end{cases}$$

$$W_{Px} = \begin{cases} 0 , & 0 < x < \ell_{P_1} \\ \dfrac{W_P(x - \ell_{P_1})}{(\ell_{P_2} - \ell_{P_1})} , & \ell_{P_1} < x < \ell_{P_2} \\ W_P , & \ell_{P_2} < x < \ell_B \end{cases}$$

$$C_{Px} = \begin{cases} 0 , & 0 < x < \ell_{P_1} \\ \dfrac{x + \ell_{P_1}}{2} , & \ell_{P_1} < x < \ell_{P_2} \\ \dfrac{\ell_{P_2} + \ell_{P_1}}{2} , & \ell_{P_2} < x < \ell_B \end{cases}$$

$$K_{Px}^2 = \begin{cases} 0 , & 0 < x < \ell_{P_1} \\ \dfrac{(x - \ell_{P_1})^2}{12} , & \ell_{P_1} < x < \ell_{P_2} \\ \dfrac{(\ell_{P_2} - \ell_{P_1})^2}{12} , & \ell_{P_2} < x < \ell_B \end{cases}$$

$$h_{L_C} = \begin{cases} 0 , & 0 < x < \ell_C \\ 1 , & \ell_C < x < \ell_B \end{cases}$$

$$h_{L_T} = \begin{cases} 0 , & 0 < x < \ell_T \\ 1 , & \ell_T < x < \ell_B \end{cases}$$

For each condition, the bending-moment distribution is then given by:

$$M_i(x) = \underset{t}{\text{MAX}} \left| M_i(x,t) \right| \tag{A3}$$

and vehicle loading by:

$$M(x) = \underset{i}{\text{MAX}} \left[M_i(x) \right] \tag{A4}$$

Only absolute values need be considered in equation (A3) because the vehicle body is symmetric about the horizontal plane.

Considering first the maneuver loading, the motion is assumed to be a static pitch-plane pull-up of given load factor n. In this case the bending-moment distribution is not time dependent. The maneuver is performed with the horizontal tail surfaces and the required angle of attack and tail deflection are given by:

$$\left.\begin{aligned} \alpha_M &= \frac{nW_M(C_M - l_T) + (C_{L_\alpha} q)_M S_C \delta_{C_M}(l_T - l_C)}{(C_{L_\alpha} q)_M \left[S_B \left(\frac{2}{3} l_B - l_T \right) + S_C(l_C - l_T) \right]} \\ \delta_{T_M} &= \frac{nW_M - (C_{L_\alpha} q)_M (S_B + S_C + S_T)\alpha_M - (C_{L_\alpha} q)_M S_C \delta_{C_M}}{(C_{L_\alpha} q)_M S_T} \end{aligned}\right\} \tag{A5}$$

The required terms in the bending-moment equation, (A2), are in this case (see assumptions stated earlier):

$$L_{B_{x_M}} = (C_{L_\alpha} q)_M \left(\frac{x}{l_B} \right)^2 S_B \alpha_M$$

$$C_{P_{x_M}} = \frac{2}{3} x$$

$$L_{C_M} = (C_{L_\alpha} q)_M S_C (\alpha_M + \delta_{C_M})$$

$$L_{T_M} = (C_{L_\alpha} q)_M S_T (\alpha_M + \delta_{T_M})$$

$$\ddot{\alpha}_M = 0 \ , \qquad \ddot{y}_M = g(n - 1) \ , \qquad N_M = 0$$

The maneuver bending-moment distribution of the nominal vehicle for a 2.5 load factor and angle of attack prior to the maneuver of 7° is shown in figure 2. The angle of attack required for the maneuver was 18°.

Next, considering the landing condition, the dynamic model used is shown in figure 16(a). The model consists of a two-degrees-of-freedom mass-spring-damper system with linear gear constants. The differential equations of the landing motion are then:

$$
\left.
\begin{aligned}
&\ddot{y}_L + \frac{g}{W_L}(h_{t_C}C_{NG} + C_{MG})\dot{y}_L + \frac{g}{W_L}(h_{t_C}K_{NG} + K_{MG})y_L \\
&+ \frac{g}{W_L}\left[h_{t_C}C_{NG}(C_L - x_{NG}) + C_{MG}(C_L - x_{MG})\right]\dot{\alpha}_L + \frac{g}{W_L}\left[h_{t_C}K_{NG}(C_L - x_{NG})\right. \\
&\left. + K_{MG}(C_L - x_{MG}) - (C_{L_\alpha}q)_L(S_C + S_B + S_L)\right]\alpha_L \\
&\qquad = \frac{g}{W_L}\left\{K_{MG}[y_{o_L} + (C_L - x_{MG})\alpha_{o_L}] + h_{t_C}K_{NG}[y_{o_L} + (C_L - x_{NG})\alpha_{o_L}]\right. \\
&\qquad\quad \left. + (C_{L_\alpha}q)_L(S_C\delta_{C_L} + S_T\delta_{T_L}) - W_L\right\} \\
&\ddot{\alpha}_L + \frac{g}{W_L K_L^2}\left[h_{t_C}C_{NG}(C_L - x_{NG})^2 + C_{MG}(C_L - x_{MG})^2\right]\dot{\alpha}_L \\
&+ \frac{g}{W_L K_L^2}\left\{h_{t_C}K_{NG}(C_L - x_{NG})^2 + K_{MG}(C_L - x_{MG})^2\right. \\
&\left. - (C_{L_\alpha}q)_L\left[S_C(C_L - \ell_C) + S_B\left(C_L - \frac{2}{3}\ell_B\right) + S_T(C_L - \ell_T)\right]\right\}\alpha_L \\
&+ \frac{g}{W_L K_L^2}\left[h_{t_C}C_{NG}(C_L - x_{NG}) + K_{MG}(C_L - x_{MG})\right]\dot{y}_L \\
&+ \frac{g}{W_L K_L^2}\left[h_{t_C}K_{NG}(C_L - x_{NG}) + K_{MG}(C_L - x_{MG})\right]y_L \\
&\qquad = \frac{g}{W_L K_L^2}\left[h_{t_C}K_{NG}(C_L - x_{NG})\right\{y_{o_L} + (C_L - x_{NG})\alpha_{o_L} + K_{MG}(C_L - x_{MG})y_{o_L} \\
&\qquad\quad + (C_L - x_{MG})\alpha_{o_L} + (C_{L_\alpha}q)_L[S_C\delta_{C_L}(C_L - \ell_C) + S_T\delta_{T_L}(C_L - \ell_T)]\}
\end{aligned}
\right\} \quad \text{(A6)}
$$

where a dot signifies a time derivative and where t_C is the time of nose gear touchdown (main gear contact occurs at $t = 0$). These equations are numerically integrated using suitable initial conditions. The required terms in the bending-moment equation are:

$$L_{Bx_L} = (C_{L_\alpha q})_L \left(\frac{x}{\ell_B}\right)^2 S_B \alpha_L$$

$$C_{Px_L} = \frac{2}{3} x$$

$$L_{C_L} = (C_{L_\alpha q})_L S_C (\alpha_L + \delta_{C_L})$$

$$L_{T_L} = (C_{L_\alpha q})_L S_T (\alpha_L + \delta_{T_L})$$

$$N_L = \begin{cases} 0, & x < x_{NG} \\ h_{t_C}(x - x_{NG}) \Big\{ K_{NG}[y_{o_L} + (C_L - x_{NG})\alpha_{o_L} - y_L - (C_L - x_{NG})\alpha_L] \\ \quad - C_{NG}[\dot{y}_L + (C_L - x_{NG})\dot{\alpha}_L] \Big\}, & x_{NG} < x < x_{MG} \\ h_{t_C}(x - x_{NG}) \Big\{ K_{NG}[y_{o_L} + (C_L - x_{NG})\alpha_{o_L} - y_L - (C_L - x_{NG})\alpha_L] \\ \quad - C_{NG}[\dot{y}_L + (C_L - x_{NG})\dot{\alpha}_L] \Big\} + (x - x_{MG}) \Big\{ K_{MG}[y_{o_L} - (C_L - x_{MG})\alpha_{o_L} - y_L + (C_L - x_{MG})\alpha_L] \\ \quad - C_{MG}[\dot{y}_L - (C_L - x_{MG})\dot{\alpha}_L] \Big\}, & x_{MG} < x < \ell \end{cases}$$

$$h_{t_C} = \begin{cases} 0, & 0 < t < t_c \\ 1, & t_c < t \end{cases}$$

The quantity N_L is the contribution of the landing gear forces to the bending moment. Figure 2 shows the landing-moment distribution of the nominal vehicle for the following initial conditions:

$$\alpha_{o_L} = 15°, \qquad \dot{\alpha}_{o_L} = 0°/\text{sec}$$

$$y_{o_L} = 9 \text{ ft}, \qquad \dot{y}_{o_L} = -V_S = -10 \text{ fps}$$

As an example of the results of an integration of the landing equations, figure 17 shows the time histories of the landing gear reactions. It was found that for this vehicle, bending moment was minimized by having relatively low damping in the main gear as compared with the nose gear. Nose gear touchdown occurred 1.75 sec after main gear touchdown and the maximum reaction occurred shortly after nose gear touchdown. The time history of the acceleration at the vehicle center of

gravity is also shown in figure 17, and the maximum value is about 23 fps^2 (1.7 load factor). Routine landings, of course, would have much lower values of acceleration.

The dynamic model for the gust loading condition is shown in figure 16(b). The vehicle, traveling with horizontal speed V, penetrates a vertical wind shear of speed V_g. This has the effect of changing the angle of attack on the portion of the vehicle that has penetrated the gust by an amount $\delta_g = V_g/V$. The equations of motion are then:

$$\left.\begin{aligned}
&\ddot{y}_G - \frac{g(C_{L_\alpha} q)_G}{W_G}(S_C + S_T + S_B)\alpha_G = \frac{g(C_{L_\alpha} q)_G}{W_G}\left[S_C(S_{C_G} + h_{t_C}\delta_g) + S_T(\delta_{T_G} + h_{t_C}\delta_g) + S_B\frac{V^2\delta_g}{l_B^2}t^2\right] - g \\
&\ddot{\alpha}_G - \frac{g(C_{L_\alpha} q)_G}{K_G^2 W_G}\left[S_C(C_G - l_C) + S_T(C_G - l_T) + S_B\left(C_G - \frac{2}{3}l_B\right)\right]\alpha_G \\
&\qquad = \frac{g(C_{L_\alpha} q)_G}{K_G^2 W_G}\left[S_C(\delta_{C_G} + h_{t_C}\delta_g)(C_G - l_C) + S_T(\delta_{T_G} + h_{t_C}\delta_g)(C_G - l_T) + \frac{S_B V^2 \delta_g C_G}{l_B^2}t^2 - \frac{2S_B V^3 \delta_g}{3l_B^2}t^3\right]
\end{aligned}\right\} \qquad \text{(A7)}$$

These equations are of the form:

$$\left.\begin{aligned}
\ddot{y}_G + A\alpha_G &= Bt^2 + H \\
\ddot{\alpha}_G + J^2\alpha_G &= Et^3 + Qt^2 + G
\end{aligned}\right\} \qquad \text{(A8)}$$

and are a system of piecewise linear, second-order, nonhomogeneous differential equations. Since the second equation is uncoupled from the first, an analytical solution is easily obtained as:

$$\left.\begin{aligned}
\alpha_G &= K_{G1}\sin(Jt) + K_{G2}\cos(Jt) + \frac{E}{J^2}t^3 + \frac{Q}{J^2}t^2 - \frac{6E}{J^4}t + \frac{G - (2Q/J^2)}{J^2} \\
y_G &= \frac{AK_{G1}}{J^2}\sin(Jt) + \frac{AK_{G2}}{J^2}\cos(Jt) - \frac{AE}{20J^2}t^5 - \left(\frac{AQ}{12J^2} - \frac{B}{12}\right)t^4 \\
&\quad + \frac{AE}{J^4}t^3 + A\left[\frac{H}{2A} - \frac{G - (2Q/J^2)}{2J^2}\right]t^2 + K_{G3}t + K_{G4}
\end{aligned}\right\} \qquad \text{(A9)}$$

where it was assumed that $J^2 > 0$ and where the constants of integration are:

$$K_{G1} = \frac{\dot{\alpha}_{o_G} + (6E/J^4)}{J}$$

$$K_{G2} = \alpha_{o_G} - \frac{G - (2Q/J^2)}{J^2}$$

$$K_{G3} = \dot{y}_{o_G} - \frac{AK_{G1}}{J}$$

$$K_{G4} = y_{o_G} - \frac{AK_{G2}}{J^2}$$

The following terms are needed for the bending-moment equation:

$$L_{Bx_G} = \begin{cases} \dfrac{(C_{L_\alpha q})_G S_B}{l_B^2}(x^2\alpha_G + V^2\delta_g t^2), & Vt < x \\ \dfrac{(C_{L_\alpha q})_G S_B}{l^2}(\alpha_G + \delta_g)x^2, & x < Vt \end{cases}$$

$$C_{Px_G} = \begin{cases} \dfrac{2(x^3\alpha_G + V^3\delta_g t^3)}{3(x^2\alpha_G + V^2\delta_g t^2)}, & Vt < x \\ \dfrac{2}{3}x, & x < Vt \end{cases}$$

$$L_{C_G} = (C_{L_\alpha q})_G S_C(\alpha_G + \delta_{C_G} + h_{t_C}\delta_g)$$

$$L_{T_G} = (C_{L_\alpha q})_G S_T(\alpha_G + \delta_{T_G} + h_{t_T}\delta_g)$$

$$N_G = 0$$

$$h_{t_C} = \begin{cases} 0 , & t < \frac{l_C}{V} \\ 1 , & \frac{l_C}{V} < t \end{cases}$$

$$h_{t_T} = \begin{cases} 0 , & t < \frac{l_T}{V} \\ 1 , & \frac{l_T}{V} < t \end{cases}$$

The bending-moment distribution due to gust loading of the nominal vehicle is shown in figure 2 for the following conditions:

$$V = 750 \text{ fps} , \qquad V_g = 50 \text{ fps}$$

$$y_{o_G} = 0 \text{ ft} , \qquad \dot{y}_{o_G} = 0 \text{ fps}$$

$$\alpha_{o_G} = 7^\circ , \qquad \dot{\alpha}_{o_G} = 0^\circ/\text{sec}$$

The time history of the acceleration of the vehicle center of gravity is shown in figure 18.

As mentioned previously, the wing-body loads are computed in a manner similar to the all-body loads. For the wing-body, static margin at cruise is specified and the wing location is determined accordingly. The wing C_{L_α} is specified independently of the body C_{L_α}. The dynamic and bending-moment equations have generally the same form as for the all-body configuration, but are slightly more complex due to the body-wing interfaces.

GTOW = 500,000 lb
Volume = 71400 ft^3
Length = 190 ft
Plan area = 9660 ft^2

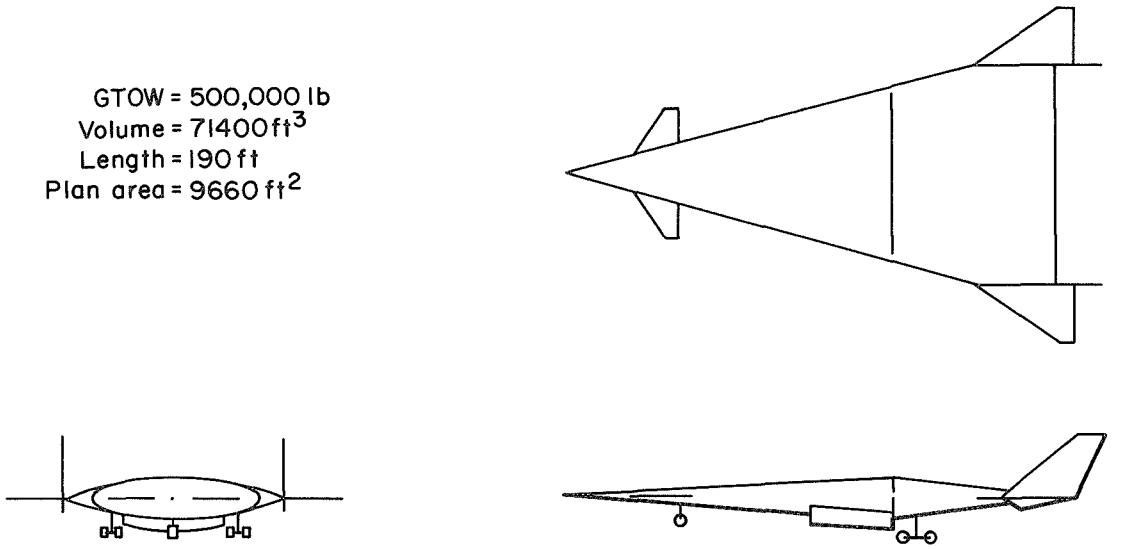

(a) All-body.

GTOW = 500,000 lb
Volume = 71400 ft^3
Length = 312 ft
Wing area = 6250 ft^3

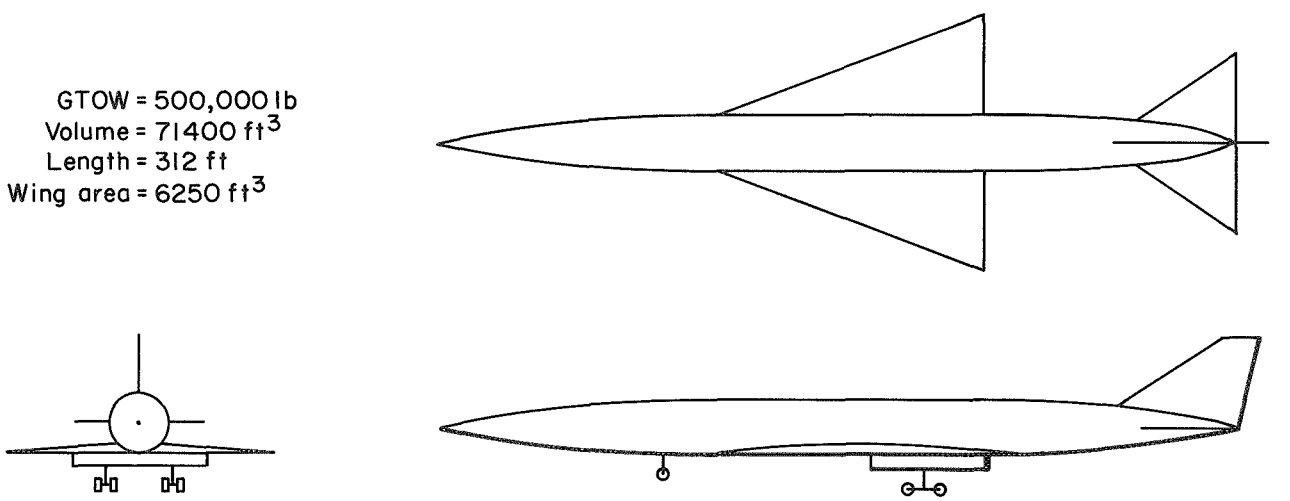

(b) Wing-body.

Figure 1.- Configurations.

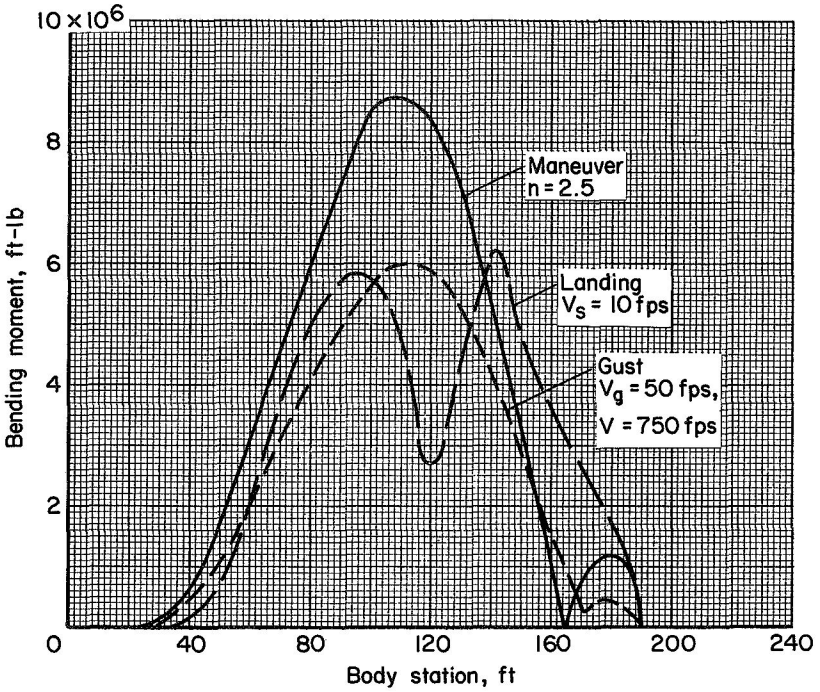

(a) All-body.

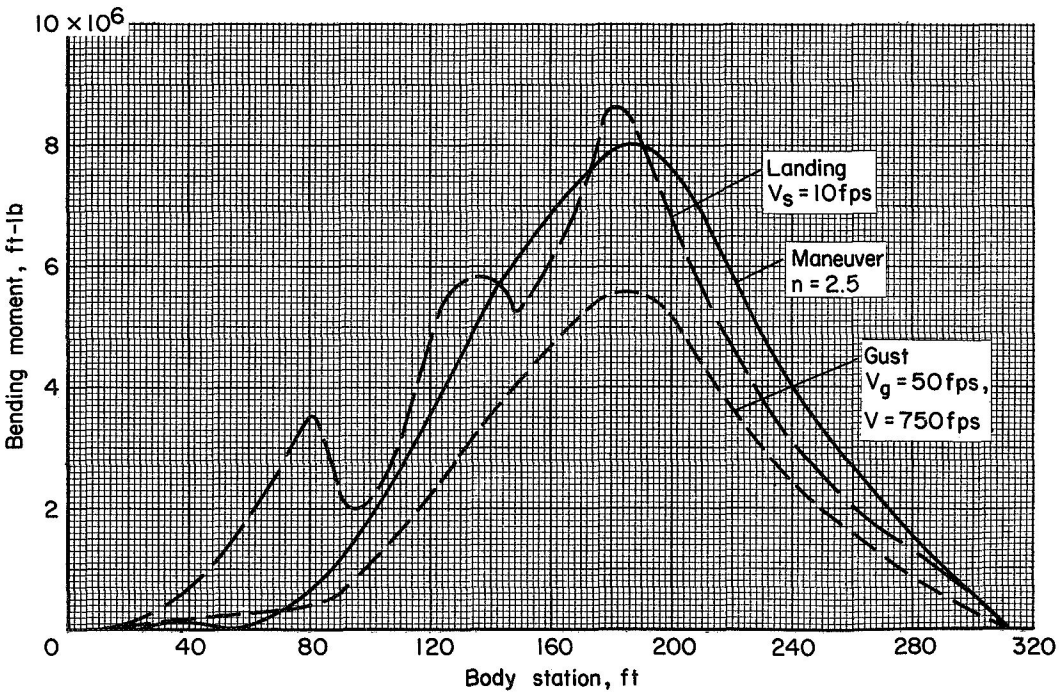

(b) Wing-body.

Figure 2.- Nominal bending moments.

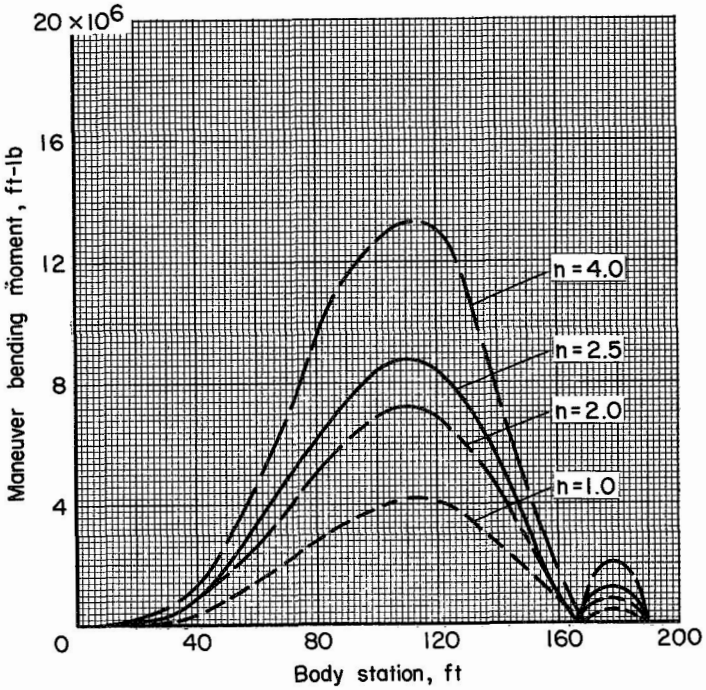

(a) All-body.

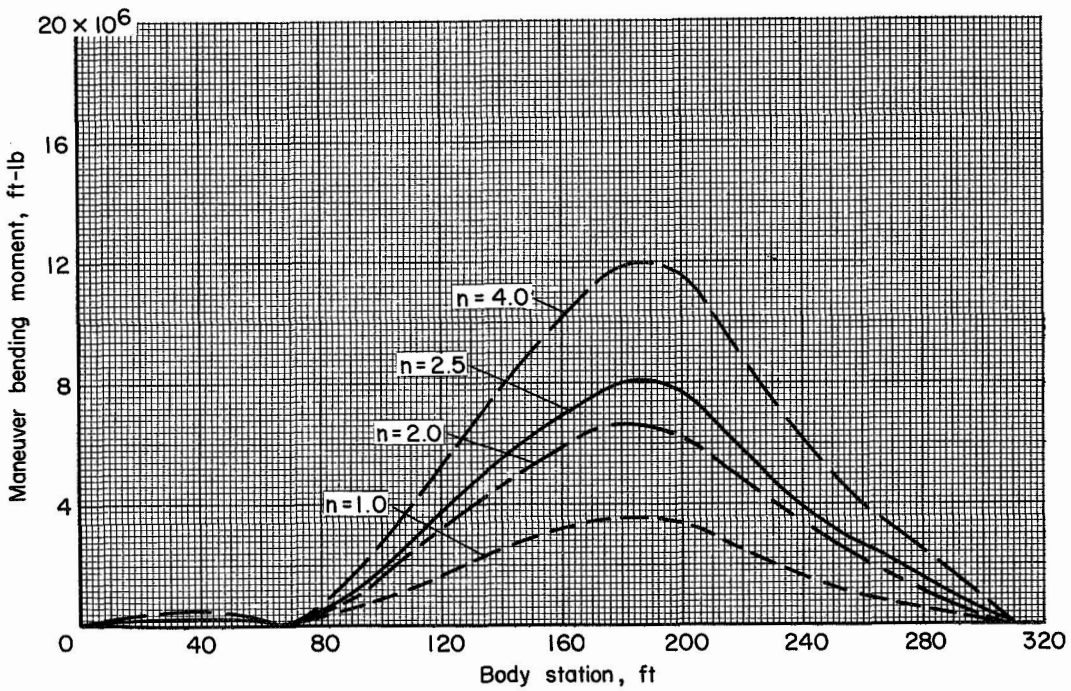

(b) Wing-body.

Figure 3.- Effect of load factor.

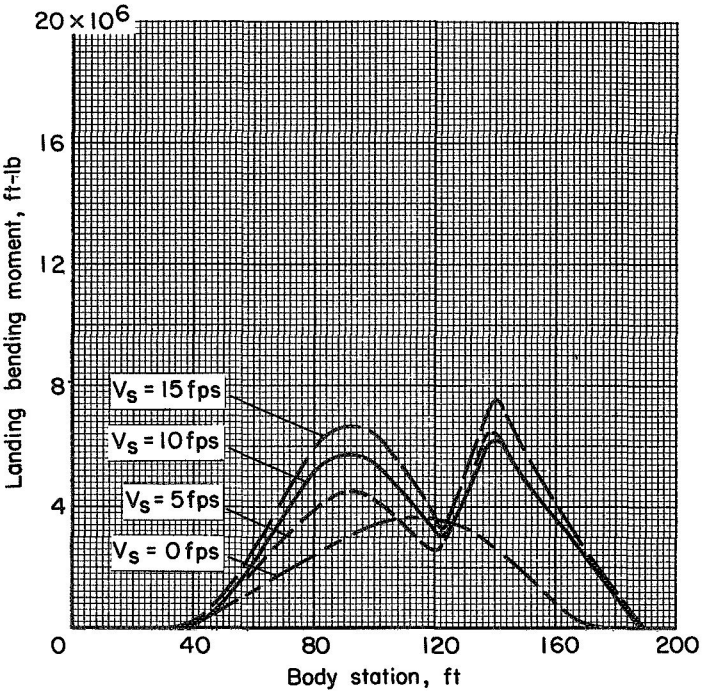

(a) All-body.

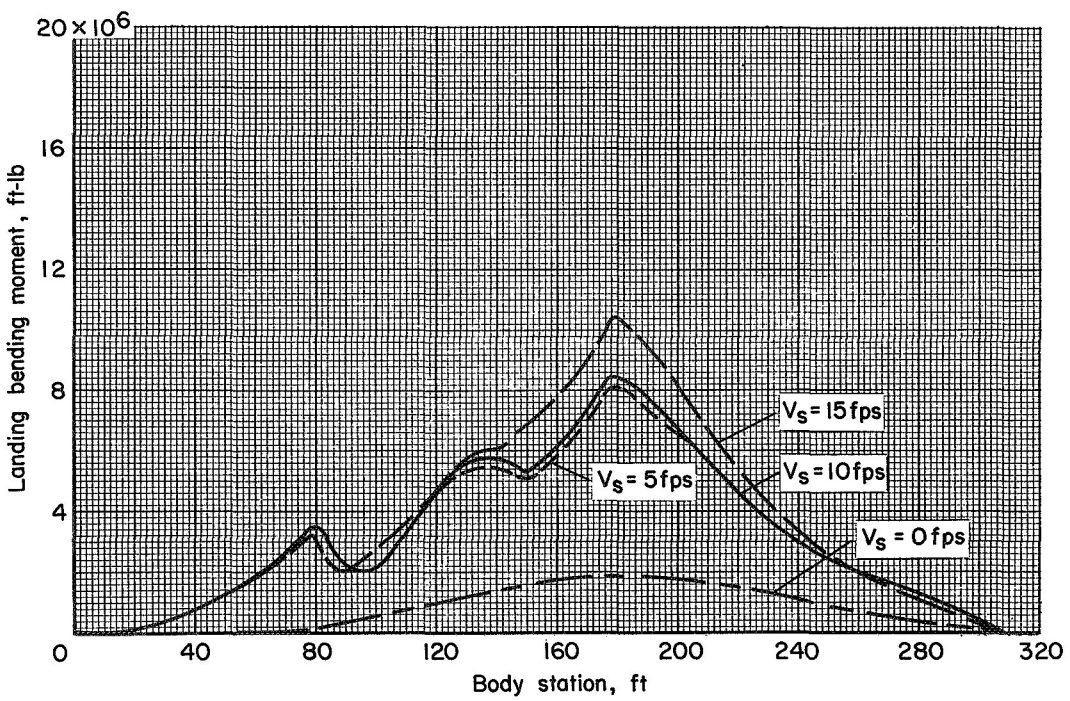

(b) Wing-body.

Figure 4.- Effect of sink speed.

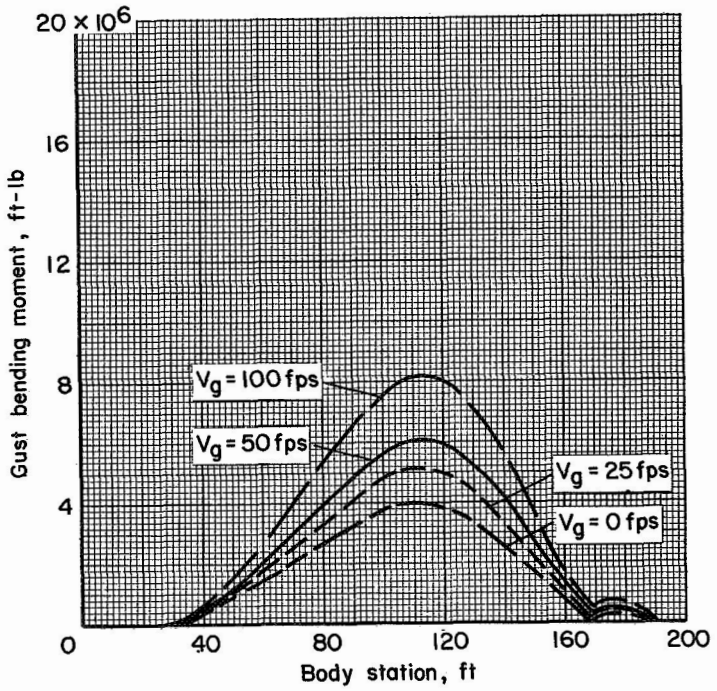

(a) All-body.

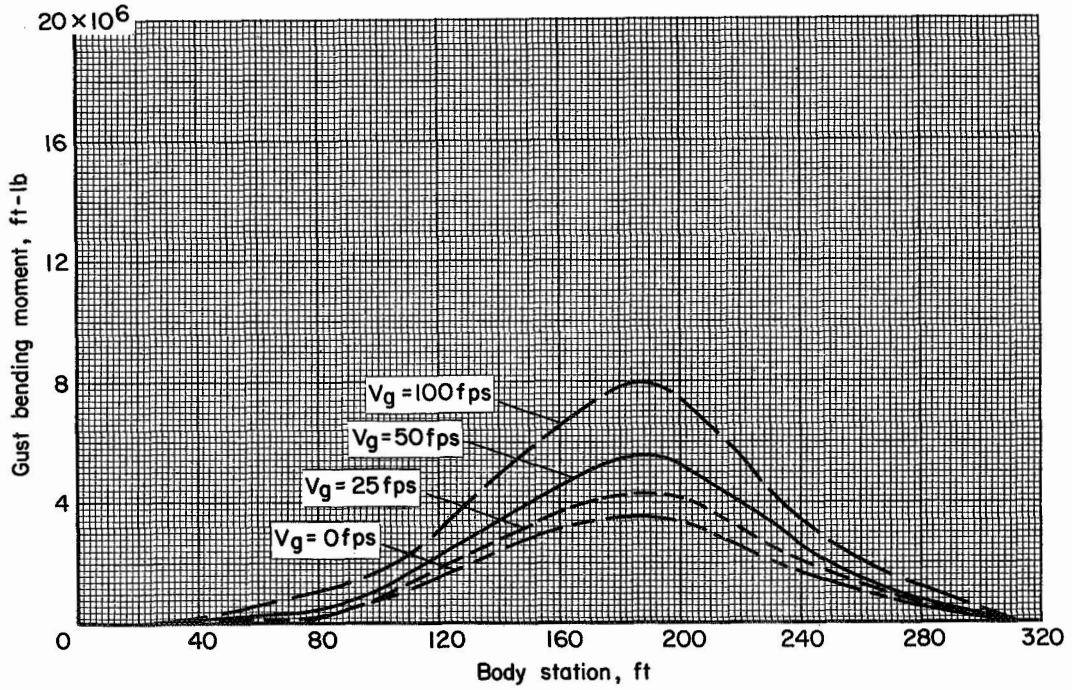

(b) Wing-body.

Figure 5.- Effect of gust velocity.

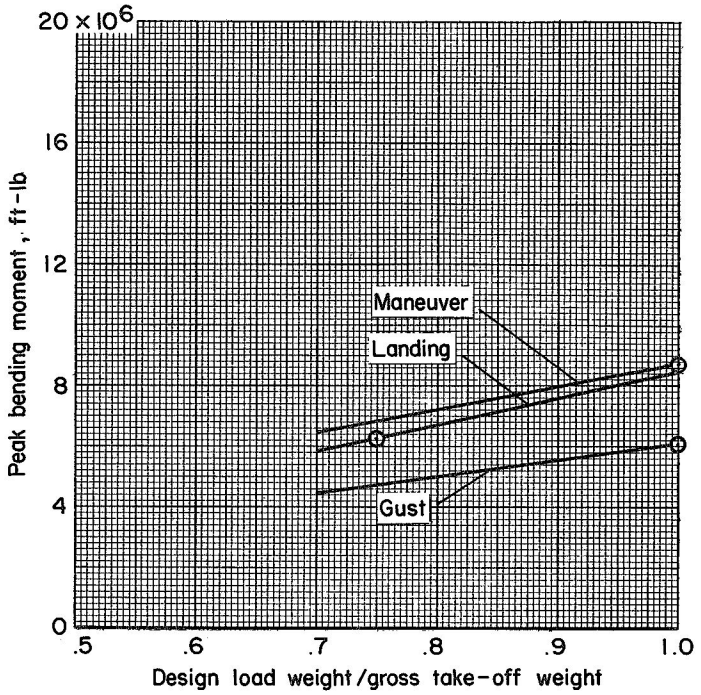

(a) All-body.

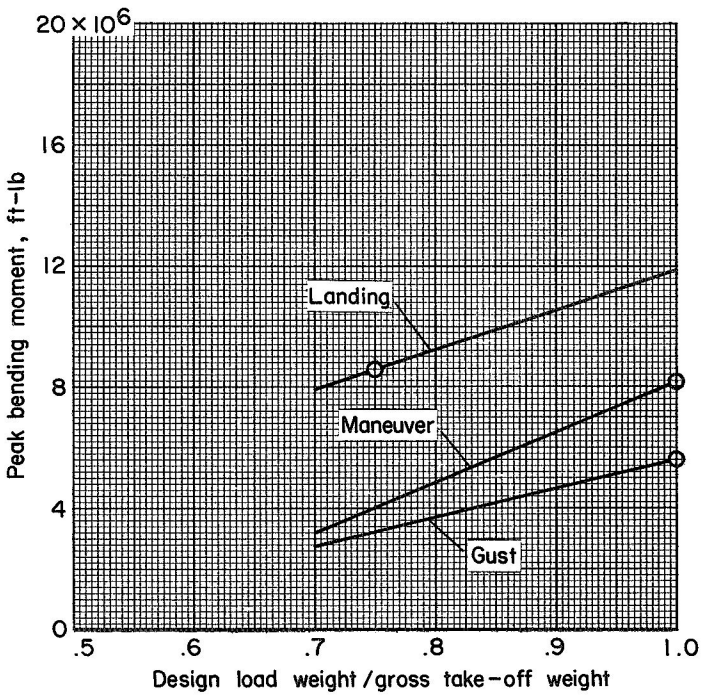

(b) Wing-body.

Figure 6.- Effect of design load weight.

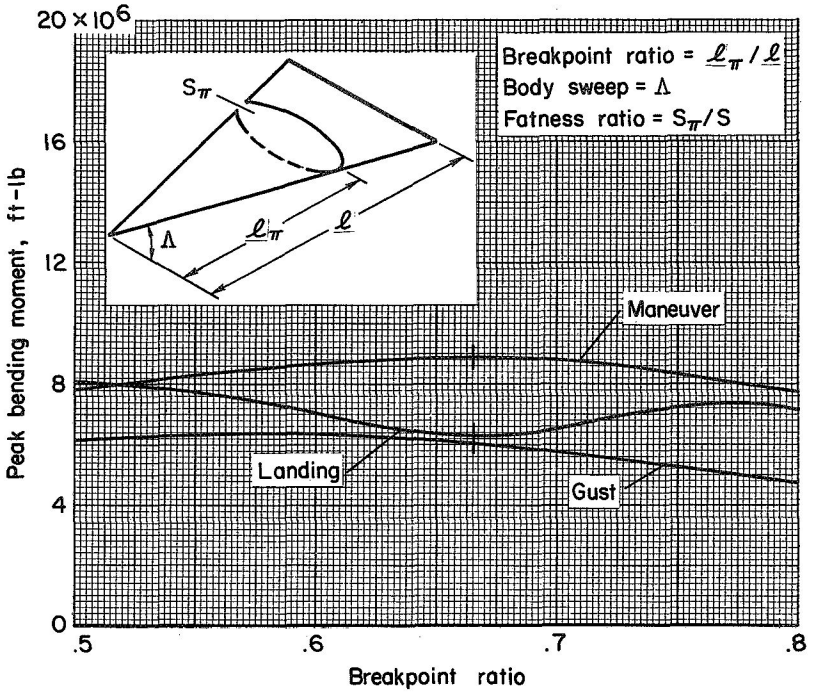

Figure 7.- Effect of breakpoint ratio, all-body.

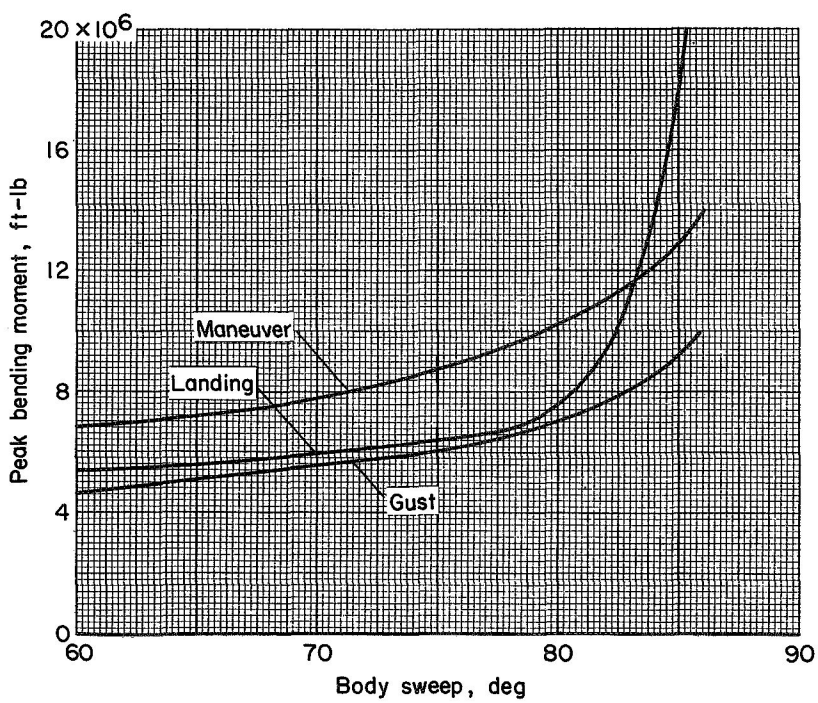

Figure 8.- Effect of body sweep, all-body.

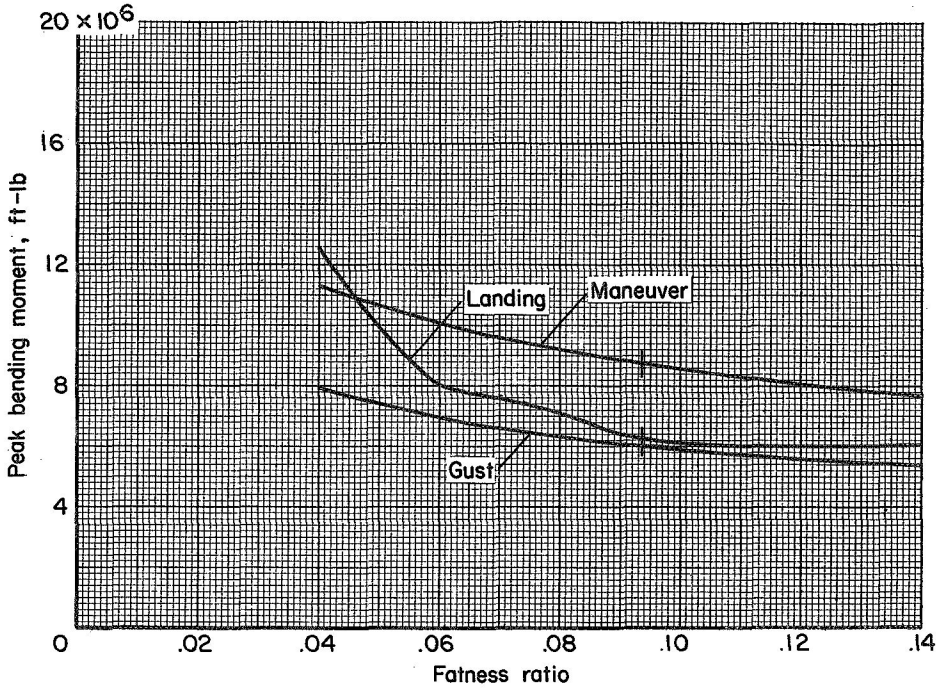

Figure 9.- Effect of fatness ratio, all-body.

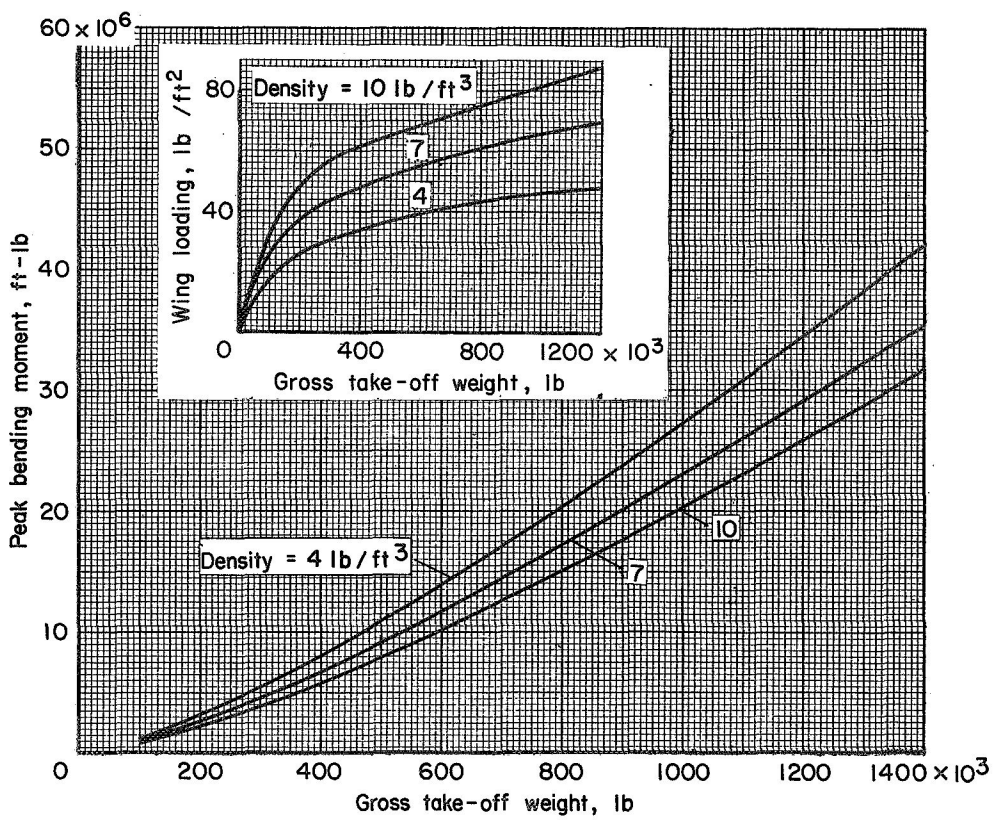

Figure 10.- Effect of size, all-body.

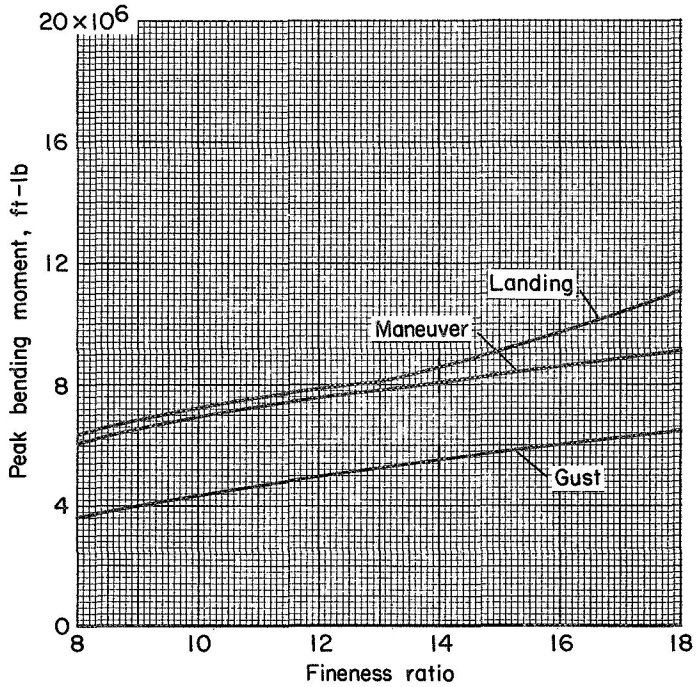

Figure 11.- Effect of fineness ratio, wing-body.

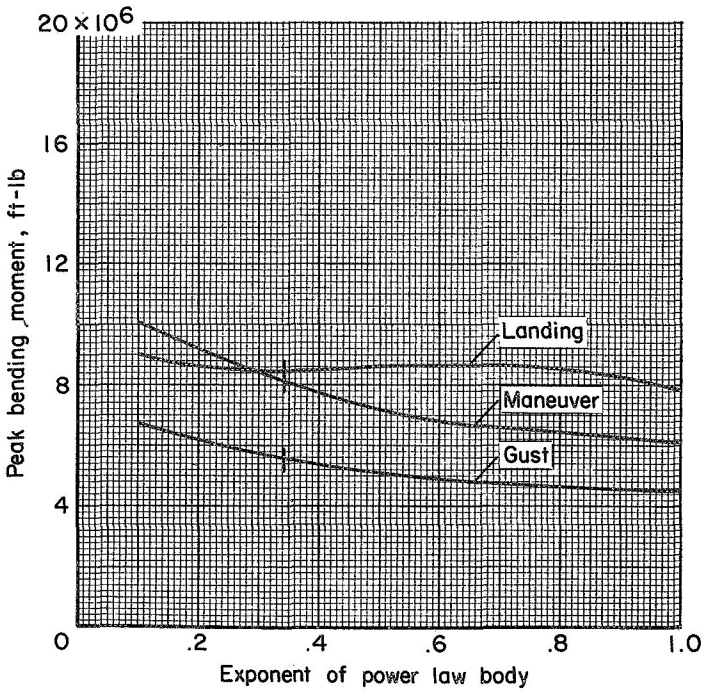

Figure 12.- Effect of exponent, wing-body.

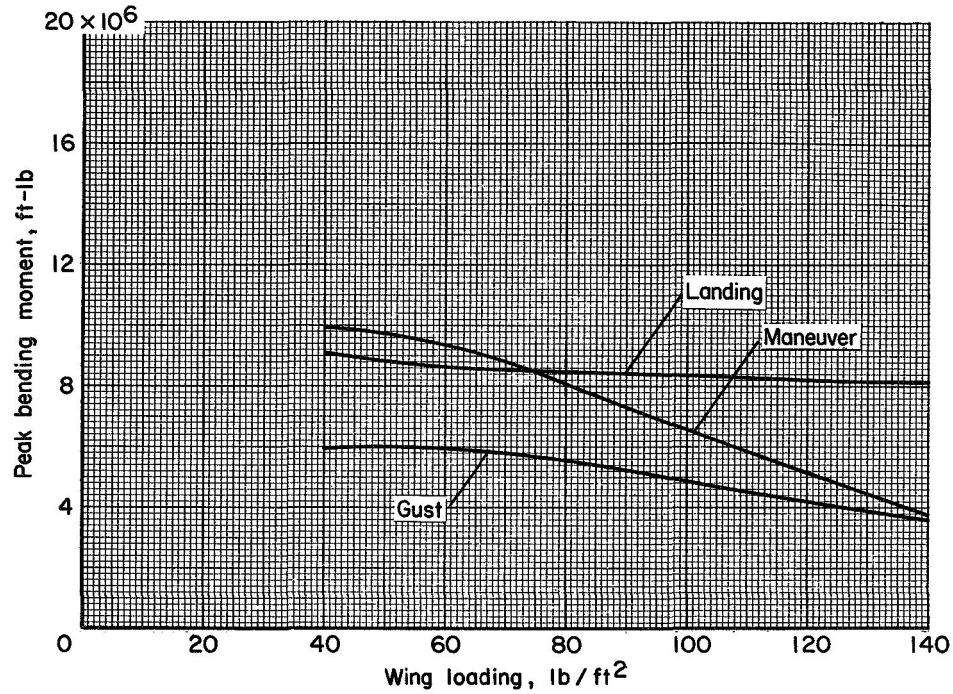

Figure 13.- Effect of wing loading, wing-body.

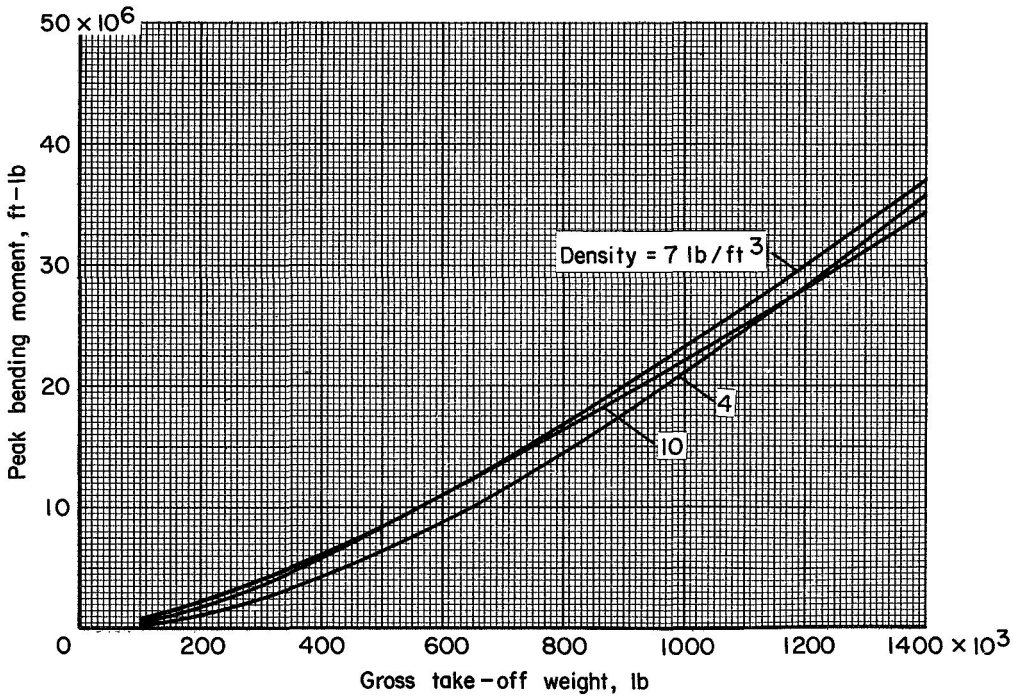

Figure 14.- Effect of size, wing-body.

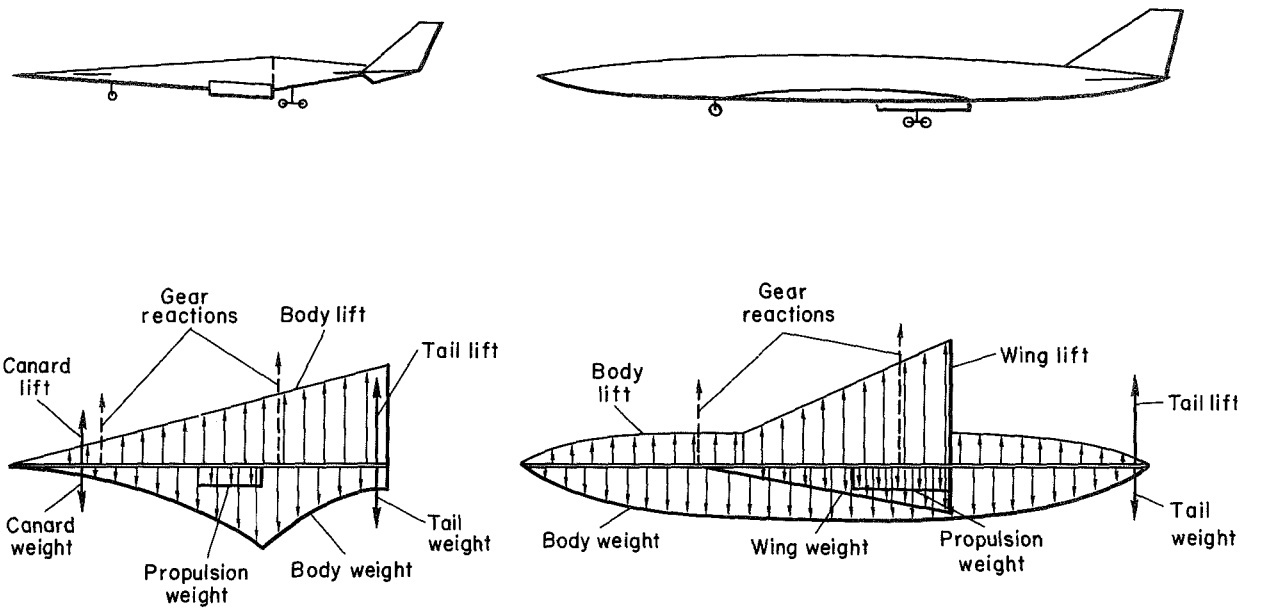

Figure 15.- Loading models.

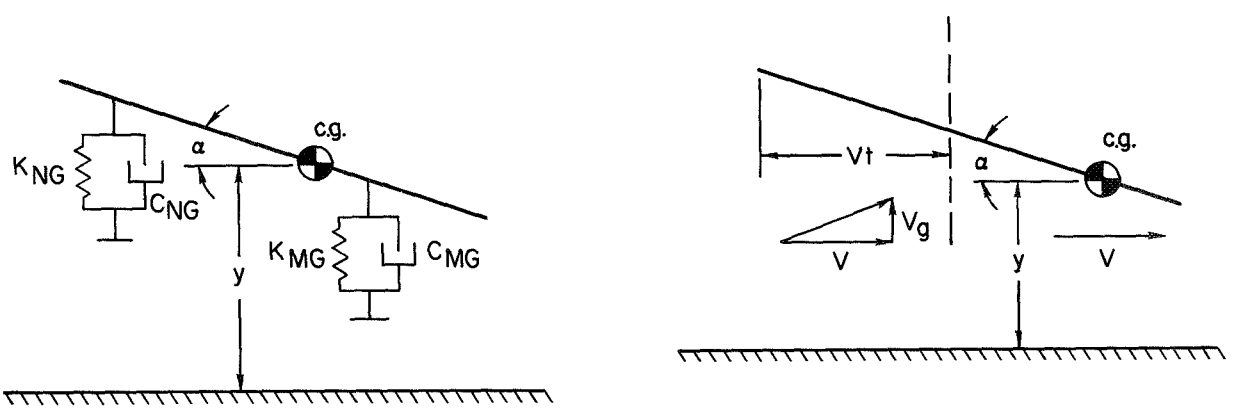

(a) Landing.

(b) Gust.

Figure 16.- Dynamic models.

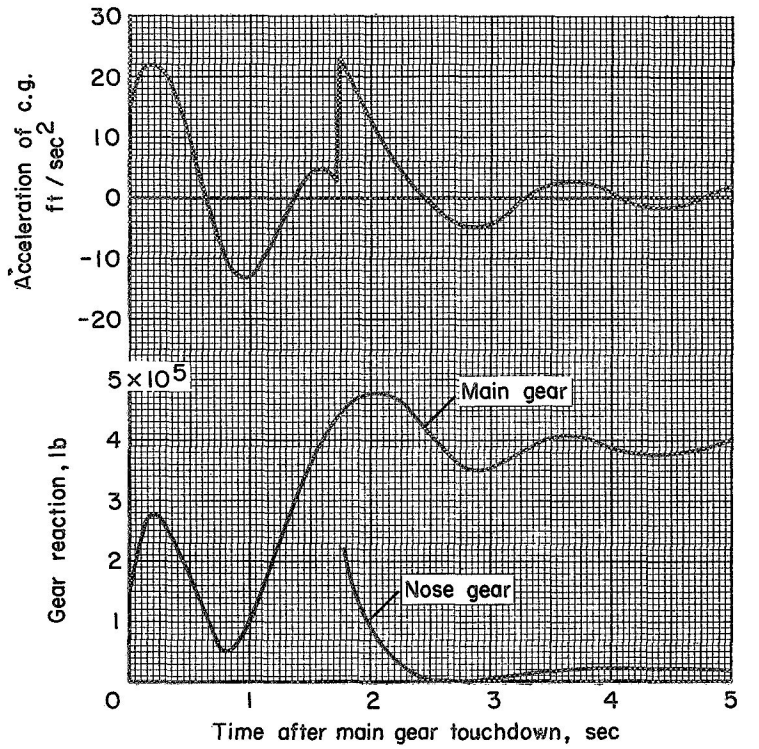

Figure 17.- Gear reactions and center-of-gravity acceleration during landing.

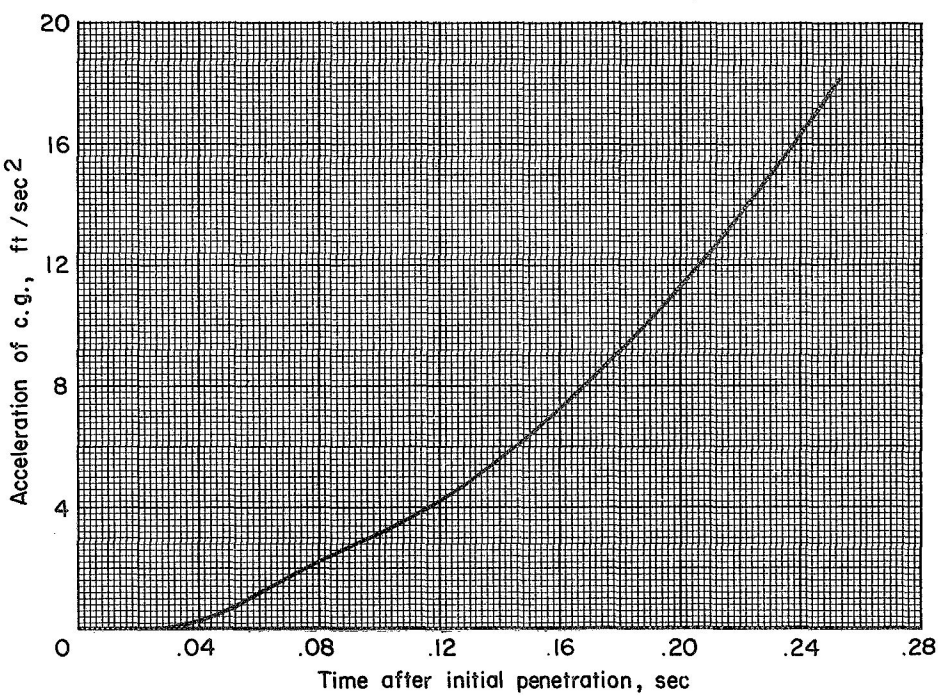

Figure 18.- Center-of-gravity acceleration during gust.

NASA-Langley, 1970 —— 32 A-3625

"The aeronautical and space activities of the United States shall be conducted so as to contribute . . . to the expansion of human knowledge of phenomena in the atmosphere and space. The Administration shall provide for the widest practicable and appropriate dissemination of information concerning its activities and the results thereof."

—NATIONAL AERONAUTICS AND SPACE ACT OF 1958

NASA SCIENTIFIC AND TECHNICAL PUBLICATIONS

TECHNICAL REPORTS: Scientific and technical information considered important, complete, and a lasting contribution to existing knowledge.

TECHNICAL NOTES: Information less broad in scope but nevertheless of importance as a contribution to existing knowledge.

TECHNICAL MEMORANDUMS: Information receiving limited distribution because of preliminary data, security classification, or other reasons.

CONTRACTOR REPORTS: Scientific and technical information generated under a NASA contract or grant and considered an important contribution to existing knowledge.

TECHNICAL TRANSLATIONS: Information published in a foreign language considered to merit NASA distribution in English.

SPECIAL PUBLICATIONS: Information derived from or of value to NASA activities. Publications include conference proceedings, monographs, data compilations, handbooks, sourcebooks, and special bibliographies.

TECHNOLOGY UTILIZATION PUBLICATIONS: Information on technology used by NASA that may be of particular interest in commercial and other non-aerospace applications. Publications include Tech Briefs, Technology Utilization Reports and Notes, and Technology Surveys.

Details on the availability of these publications may be obtained from:

SCIENTIFIC AND TECHNICAL INFORMATION DIVISION

NATIONAL AERONAUTICS AND SPACE ADMINISTRATION

Washington, D.C. 20546